Journal of Photochemistry and Photobiology A: Chemistry 214 (2010) 248–256

Contents lists available at ScienceDirect

Journal of Photochemistry and Photobiology A: Chemistry

journal homepage: www.elsevier.com/locate/jphotochem

Room temperature anthracene excimer emission from self-assembled (aminomethyl)anthracene derivatives in plastic crystalline phase

M. Jaseer, Edamana Prasad*

Department of Chemistry, Indian Institute of Technology Madras (IITM), Chennai 600 036, India

ARTICLE INFO

Article history:
Received 24 March 2010
Received in revised form 26 June 2010
Accepted 2 July 2010
Available online 31 July 2010

Keywords:
Excimer emission
Plastic crystal
Self-assembly
Silver nanoparticle
Luminescence

ABSTRACT

A series of (aminomethyl)anthracene (**AMA**) derivatives with single alkyl chain substituent (octyl, dodecyl, octadecyl and *p*-butylaniline) were synthesized and self-assembly of the compounds was analyzed in dichloromethane and solid thin film. Upon heat treatment of the solid thin films, the **AMA** derivatives exhibit plastic crystalline phase which can be preserved in a glassy state through rapid cooling of the system to room temperature. In the glassy state, the **AMA** derivatives are arranged in rectangular discotic columnar fashion, where the face-to-face distance between two anthracene moieties is 3.9 Å. Steady state and time resolved fluorescence studies were carried out in dichloromethane, which indicate that a fraction of the **AMA** derivatives form anthracene excimer, upon excitation at 360 nm. Conversely, photoexcitation of the solid thin film at 360 nm leads to the exclusive formation of anthracene excimers due to the close proximity of anthracene units in the discotic columnar arrangement. Furthermore, the self-assembled **AMA** derivatives were utilized as effective templates for in situ prepared Ag nanoparticles. While the **AMA** derivatives stabilize the Ag nanoparticles effectively, the excimer emission intensity was quenched in the presence of silver nanoparticles. The experimental results from the present study provide a unique approach for generating anthracene excimer emission from solid thin films at room temperature, which is a rare observation.

1. Introduction

Utilizing small organic molecules to generate highly hierarchical and self-assembled systems is an area of research which is gaining increasing attention among material chemists [1–3]. Identifying interesting material properties in self-assembled systems composed of small organic molecules is largely appealing because: (a) they are relatively easy to synthesize and characterize unambiguously, (b) they are less complex when handling for device fabrication, and (c) they resemble to many in vivo systems in terms of numerous aspects of self-assembly [4–7].

Anthracene derivatives play a pivotal role in the design of luminescent materials, with wide applications in lasers, phosphors, and light emitting devices [8–12]. Anthracene derivatives are also known for their [4+4] cycloaddition reactions as well as excimer formation [13–21]. It has been reported in the literature that anthracene generally form two types of excimers with slightly different geometry in the excited state [22]. The first one, where two anthracene units overlap at an angle of 55° to each other, is relatively stable and has a short excited state lifetime (<10 ns) with an emission maximum close to 470 nm [22]. The second one involves the formation of 'sandwich type' excimer where the two anthracene units are symmetrically π-stacked and such excimers exhibit longer lifetimes at lower temperatures with an emission maxima at 560 nm [22]. A recent report suggests the formation of another type of anthracene excimer (T-shaped excimer) with an emission maximum at 510 nm and an excited state lifetime of ~20 ns [23]. Although the planar structure of anthracene is quite favorable for excimer formation on photoexcitation, the excimer emission from anthracene-based systems is rarely reported, especially at room temperature [11]. Herein we report the generation of highly emitting anthracene excimers at room temperature from a series of amino(methylanthracene) (**AMA**) derivatives.

(Aminomethyl)anthracene derivatives have been well studied for their luminescence and charge transfer properties [24]. However, the self-assembling property of these small organic molecules has not been explored in detail. We have identified that, upon heat treatment, the **AMA** derivatives (compounds **C8-I**, **C12-II**, **C18-III** and **PhC4-IV** shown in Chart 1) self-assemble to rectangular discotic columnar structures, where the anthracene units are placed in close proximity to each other. We have also identified that the self-assembly at elevated temperatures renders plastic crystalline behavior to the **AMA** derivatives. The plastic crystalline properties are originated from the free rotation of lattice points, often

* Corresponding author. Tel.: +91 44 2257 4232; fax: +91 44 2257 4202.
E-mail address: pre@iitm.ac.in (E. Prasad).

1010-6030/$ – see front matter © 2010 Elsevier B.V. All rights reserved.
doi:10.1016/j.jphotochem.2010.07.003

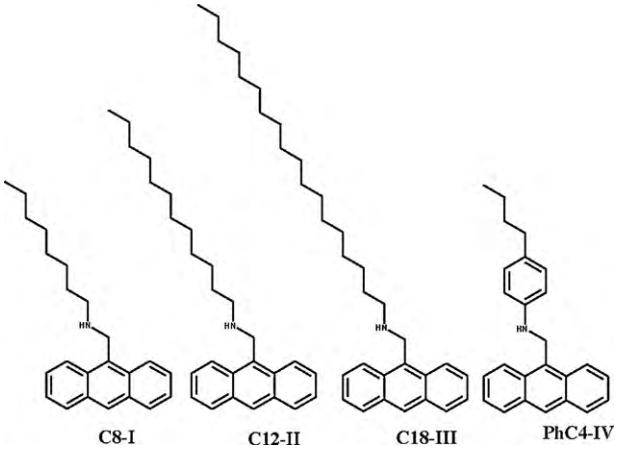

Chart 1. Structure of compounds used in the present study.

at elevated temperatures, keeping their centre of mass at ordered sites in the crystalline lattice [25]. The plastic crystalline phase of the compounds was characterized through X-ray diffraction and OPM studies. Since the plastic crystalline phase was preserved in a glassy state upon rapid cooling of the system from the isotropization point to room temperature, anthracene excimers were readily formed in the glassy state of the **AMA** derivatives. The **AMA** derivatives were also utilized for in situ generation and stabilization of silver nanoparticles and the effect of Ag nano-guest molecules on the excimer emission intensity was investigated in the solid thin films. The mechanistic studies suggest that controlling the self-assembling property of the **AMA** derivatives provides a unique approach for generating intense anthracene excimer emission at room temperature.

2. Experimental

2.1. Materials

9-Anthraldehyde and 4-butylaniline were purchased from Aldrich chemical company, USA. Octadecylamine, dodecylamine, octylamine and silver nitrate were purchased from Sd Fine Chemicals, India and the amines were purified through distillation under reduced pressure.

2.2. Synthesis of 9-(p-butylphenylaminomethyl) anthracene (*PhC4-IV*)

In a typical procedure, a solution of 9-anthraldehyde (0.1 g, 0.48 mmol) in ethanol (20 mL) was added drop-by-drop to a solution of *p*-butylaniline (0.076 g, 0.48 mmol) dissolved in ethanol (5 mL). The mixture was stirred under reflux condition for 12 h. The reaction mixture was allowed to cool to room temperature. To the imine formed, solid $NaBH_4$ (0.02 g, 0.58 mmol) was added in portions and the stirring was continued for another 12 h. The reaction mixture was evaporated to dryness, extracted with ether and purified by column chromatography (silica gel, hexane/ethyl acetate 10:1) to give 9-(*p*-butylphenylaminomethyl)anthracene (**PhC4-IV**) (0.10 g, 62%) as a pale yellow solid.

^{1}H NMR (400 MHz, CDCl3) δ: 8.4 (1H, s), 8.22 (2H, d), 7.96 (2H, d), 7.55 (2H, t), 7.43 (5H, q), 7.04 (2H, d), 6.69 (3H, t), 5.07 (1H, s), 2.51 (2H, t), 2.1 (2H, s), 1.54 (2H, q), 1.31 (2H, q), 0.88 (3H, t). Mass (ESI): calculated for $C_{25}H_{25}N$. 339; found 338 (M–H), 191 (Ar–CH_2).

The procedures for synthesizing other compounds (**C8-I**, **C12-II**, and **C18-III**) as well as the spectral data are given in Supporting information.

2.3. In situ generation of silver nanoparticles

In a typical procedure, solid $AgNO_3$ (0.002 g, 0.01 mmol) was added in portions to a solution of **C18-III** (0.03 g, 0.05 mmol) in dry methanol (10 mL), and the mixture was stirred in a dark chamber for 24 h at room temperature, to get a clear solution, which is slightly reddish brown in color. The solution was drop cast on a glass slide and another glass slide was gently pressed on the top of it to form a thin film in between the glass plates. The heat-treated glass plate was then examined through POM.

2.4. Instruments

UV–visible absorption spectra were recorded on a Perkin Elmer Lambda 25 UV–visible spectrophotometer. Luminescence experiments were carried out using HORIBA JOBIN YVON Fluoromax 4 spectrometer. The lifetime studies were conducted using the Time Correlated Single Photon Counting technique (TCSPC) with microchannel plate photomultiplier tube (MCP-PMT) as detector and nanosecond LED as the excitation source (model Fluorocube, Horiba Jobin Yvon). The optical textures of the mesophases were studied using Nikon Eclipse LV 100 POL polarizing optical microscope (POM) attached with a heating and cooling stage. The transition temperatures and change in enthalpy for phase transitions were determined by differential scanning calorimetry (DSC) with NETZSCH DSC 204 instrument operated at a scanning rate of 5 °C/min. Transmission electron microscopy (TEM) images of the nano-silver were taken using a FEI Tecnai G2 30 S-TWIN, operated at 300 kV and JEM 3010 JEOL, operated at 200 kV. Scanning electron microscopy (SEM) images were taken using FEI; QUANTA scanning electron microscope. The X-ray measurements were performed using Cu Kα radiations (l = 1.5418 Å) from a fine focus sealed-tube generator in conjunction with double mirror focusing optics.

3. Results and discussion

3.1. Identifying plasticity in the *AMA* derivatives

The structure of the four (aminomethyl)anthracene derivatives used in the present study is given in Chart 1. The compounds **C8-I** and **C12-II** were reported in the literature [26,27]. However, no mesophase properties were investigated for these compounds. Compounds **C18-III** and **PhC4-IV** were synthesized adopting the procedure for **C8-I** with necessary modification.

Polarization optical microscopy is a powerful tool to understand the morphology of molecular assembly in the solid state as well as liquid crystalline state. The POM image of **C12-II** is given in Fig. 1 which showed the characteristic features of spherulitic texture, indicating the presence of discotic columnar arrangement in the system [28–30].

The POM image was taken after the heat treatment of the sample on a glass slide above the melting point (78.2 °C) followed by sudden cooling to room temperature. The POM images of **C8-I**, **C18-III** and **PhC4-IV** also exhibited similar discotic columnar arrangements in the respective systems (please see Supporting information Figs. S1–S3).

Differential scanning calorimetry (DSC) experiments were performed in order to understand the thermodynamic properties of the phase transitions in the systems upon heat treatment. Fig. 2 shows the DSC thermograms of the compounds **C8-I**, **C12-II**, **C18-III** and **PhC4-IV**, all of which show two thermodynamic transitions during the heating scan. The first peak indicates transition from the crystal phase to mesophase and the second peak corresponds to the melting of the mesophases to isotropic liquid.

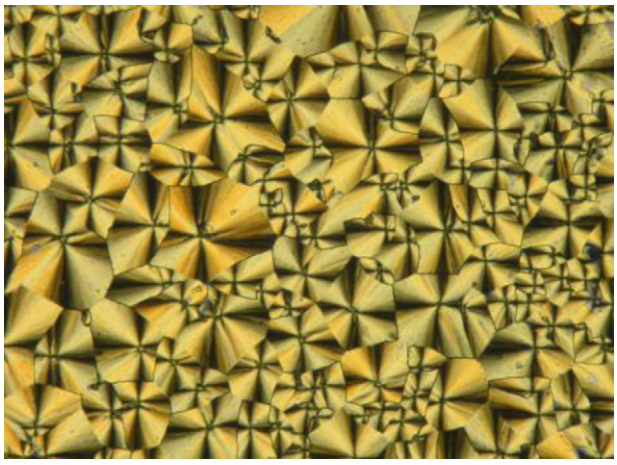

Fig. 1. POM image of **C12-II** (magnification 20×). Sample for POM was prepared by making thin film of **C12-II** (0.010 g, 0.03 mmol) in between two glass slides. The film was made uniform by heating the sample to melting followed by rapid cooling to room temperature.

In the case of **C8-I**, the crystalline phase transforms into mesophase upon heating at 72.39 °C and the system isotropizes on further heating up to 88.4 °C. The temperature range where compounds exhibit the mesogenic property (phase II) was very narrow for **C12-II** and relatively wide for **PhC4-IV**. The entropy change for the phase I–II transition increases by an order of magnitude along the series from **C8-I** to **C18-III** (0.004–0.04 J K^{-1} mol^{-1}). Interestingly, the transition temperature from phase II to III decreases as the alkyl chain length increases (from 88.4 to 73.2 °C), except for **PhC4-IV**. In the case of both transitions (from phase I to II as well as from II to III) the compound **PhC4-IV** shows relatively less entropy change, due to the strong hydrophobic interactions between the aromatic units in the molecular packing, which is consistent with the increased transition temperature from phase II to phase III (115.3 °C). The phase transition temperatures as well as thermodynamic parameters associated with the transition are summarized in Table S1 in Supporting information.

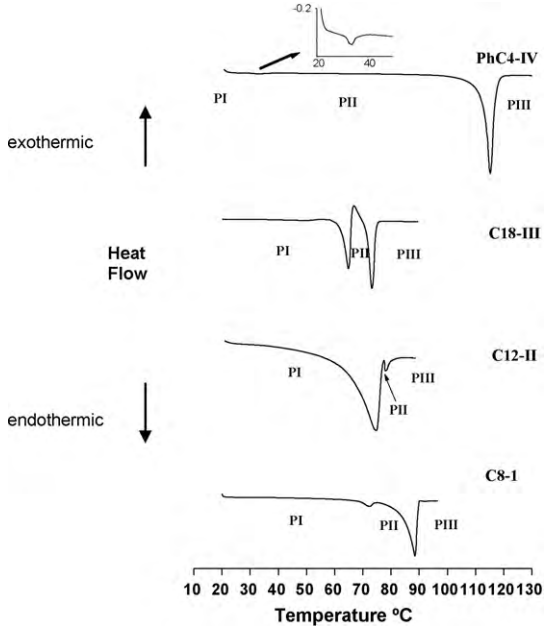

Fig. 2. DSC thermograms of the plastic crystalline compounds (all second heating cycle with a heating rate of 5°/min). PI = crystalline phase, PII = mesophase and PIII = isotropic phase.

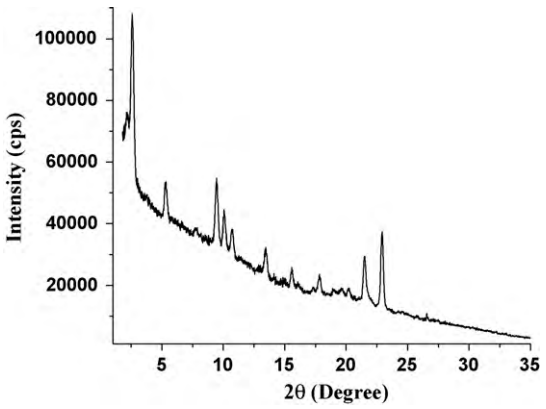

Fig. 3. XRD pattern of **C18-III** at 36.7 °C after melting and cooling in a similar procedure adopted for POM studies.

While the POM images and DSC diagrams clearly suggest the presence of mesophase with texture properties similar to discotic columnar arrangement, X-ray diffraction (XRD) studies were performed to confirm the plastic crystalline property of the **AMA** derivatives. The XRD pattern for the compound **C18-III** is given in Fig. 3. The sample was heated above the melting point (73.23 °C) mounted in a variable temperature XRD facility and the XRD pattern was recorded after cooling of the sample close to room temperatures (36.7 °C).

The presence of very sharp peaks in wide-angle region of intensity vs. 2θ profile typically confirms the presence of plastic crystalline nature of the material [30]. It is noteworthy that the entropy of fusion for the compounds obtained from DSC analysis is also consistent with Timmerman's criteria for plastic crystalline system (i.e., considerably less than 20 J K^{-1} mol^{-1}) [31]. Since POM images clearly indicate the columnar discotic type arrangement in the system, XRD pattern was further analyzed to understand whether rectangular or hexagonal type discotic arrangement is present in the plastic crystal. In the case of rectangular symmetry, the lattice parameter 'a' should satisfy the relation

$$a = 2d_{(20)},$$

whereas for hexagonally symmetric systems, the lattice parameter should be in consistent with the relation

$$a = \frac{2}{\sqrt{3}} d_{(10)},$$

where d is the inter planar distance [32]. For rectangular columnar phases, d can be calculated using the expression

$$\frac{1}{d_{(hk)}} = \sqrt{\frac{h^2}{a^2} + \frac{k^2}{b^2}}$$

where h and k are the Miller indices and a and b are lattice parameters [32]. The XRD pattern of **C18-III** strictly satisfied the requirement for rectangular symmetry (a = 68.11 and d = 34.05, from experiment) (please see Supporting information, Table S2 for XRD details). Thus, based on the XRD results for **C18-III**, it can be concluded that the **AMA** derivatives exhibit plastic crystalline behavior with rectangular columnar arrangement.

While organic molecules form discotic type arrangement when they contain usually 3 or 4 alkyl or alkoxy groups, the present case provides an exceptional example, most likely due to the presence of anthracene moiety, which occupies most of the volume of the 'disc', which otherwise is occupied by the multialkyl chains present in the system [30]. The initial report on the crystal structure of

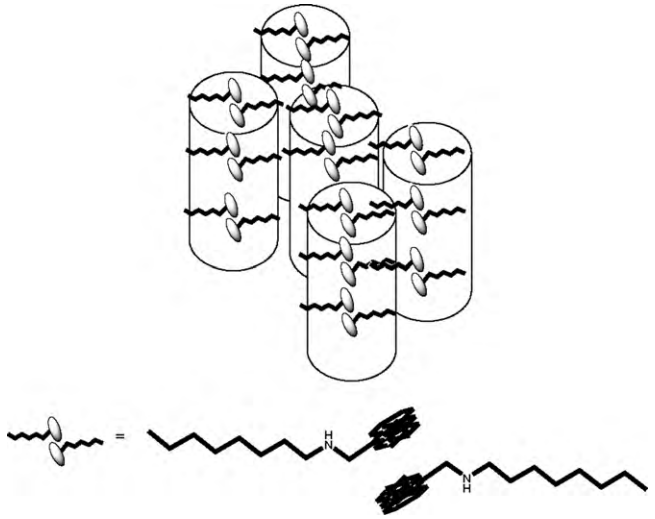

Chart 2. Cartoon representation showing the rectangular columnar arrangement in **C8-I**.

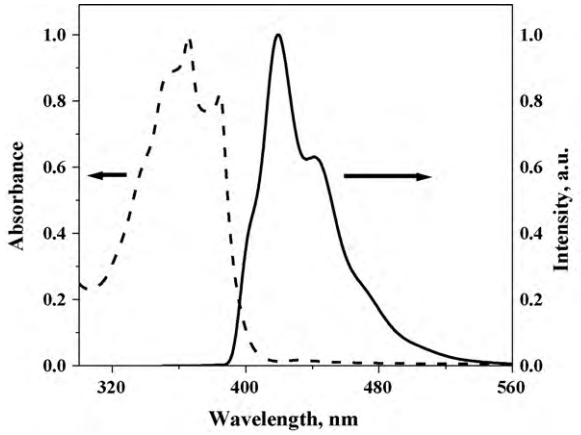

Fig. 4. UV–visible absorption and steady state emission spectra of **C8-I** (1×10^{-3} M) in dichloromethane. The excitation wavelength was 360 nm.

C8-II described a 'zig-zag' arrangement of the molecules in the crystal lattice with orthorhombic unit cell arrangement [27]. However, upon heat treatment the self-assembling propensity of the molecules is changed, which is not uncommon for systems containing anthracene units. For example, the recent report by Ziessel and co-workers describe the self-assembly of ionic liquid crystals containing anthracene core, where the zig-zag arrangement of the crystal lattice is altered to hexagonal columnar phase upon heat treatment [33].

The π–π interaction between the aromatic moieties as well as the hydrogen bonding between the amine groups could lead to columnar disc like arrangements of the compounds, which easily stack in to three-dimensional rectangular geometry as schematically shown in Chart 2. The POM images of all the compounds exhibit identical type textures, indicating that rectangular columnar arrangement is present in all the systems examined in this study.

The minimum energy configuration for a pair of **C8-I** molecules in the face-to-face geometry was obtained through the MM2 computations of the Chem. 3D pro., which suggests the stacking of the two aromatic units one over the other, with the alkyl chains stretching towards either sides. The distance between two anthracene units, which are placed one over the other was 3.87 Å in the minimum energy configuration. This was consistent with the XRD data obtained for the compound (entry 15 in Table S2 in Supporting information).

3.2. Photophysical properties of the plastic crystalline molecules in dichloromethane

Since the anthracene units are arranged in close proximity in the self-assembled **AMA** derivatives, we explore the likelihood of the anthracene excimer formation in solution, upon photoexcitation. The photophysical properties of compounds **C8-I**, **C12-II**, **C18-III** and **PhC4-IV** were initially examined in dichloromethane, since the compounds were highly soluble in dichloromethane.

The absorption and emission spectra of the **AMA** derivatives were identical to that of anthracene when the concentration of the solution was 10^{-5} M. The quantum yields of emission from **C8-I**, **C12-II**, **C18-III** to **PhC4-IV** in dichloromethane were determined using coumarin as standard and the values are summarized in Table 1. The **AMA** derivatives exhibit emission quantum yield slightly less than that of pure anthracene. However, increase in the concentration by two orders of magnitude resulted in interesting changes in the photophysical properties. Fig. 4 shows the absorption and steady state emission spectra of **C8-I** in dichloromethane, where the concentration of **C8-I** was 10^{-3} M. The steady state emission spectrum of the **C8-I** was similar to that of anthracene emission spectrum at this concentration also. However, a less intense, but broad shoulder band on the longer wavelength region was observed, which indicates that a fraction of monomer anthracene units in the **AMA** derivative forms excimers upon excitation.

The excimer formation from the **AMA** derivatives in dichloromethane at higher concentration was further confirmed thorough time resolved experiments. The time resolved fluorescence decays of compounds **C8-I**, **C18-III** and **PhC4-IV** were biexponential whereas that of **C12-II** was triexponential in dichloromethane. Fig. 5 contains the fluorescence decay of **C8-I** (please see Supporting information Figs. S4–S6 for the fluores-

Table 1
The photophysical properties of **C8-I**, **C12-II**, **C18-III** and **PhC4-IV** in dichloromethane.

Compound	Absorption maxima, nm	Emission maxima, nm	Emission quantum yield[a]	τ, ns (relative amplitude, %)
C8-I	262, 357 365, 384	420, 442, 472	0.26	$\tau_1 = 3.52\,(22.34)$ $\tau_2 = 7.46\,(77.66)$
C12-II	264, 355 366, 384	420, 444, 474	0.22	$\tau_1 = 2.78\,(33.79)$ $\tau_2 = 5.56\,(04.76)$ $\tau_3 = 11.10\,(61.44)$
C18-III	264, 355 365, 382	418, 442, 471	0.16	$\tau_1 = 2.72\,(19.12)$ $\tau_2 = 7.28\,(80.88)$
PhC4-IV	263, 356 364, 384	420, 443, 473	0.33	$\tau_1 = 2.31\,(32.89)$ $\tau_2 = 7.07\,(67.11)$

[a] Emission quantum yield of plastic crystals were determined using Coumarin as standard. Error bar is ±5%.

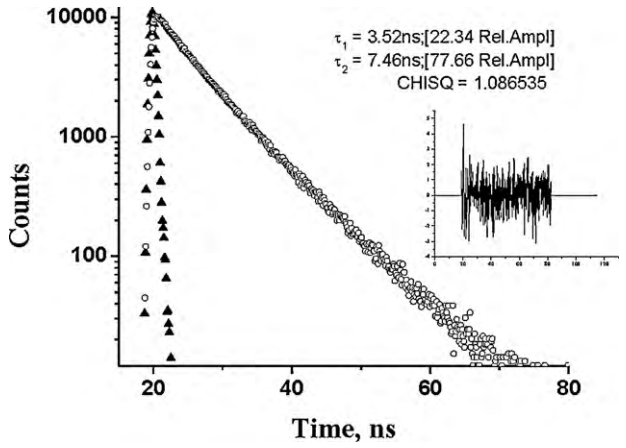

Fig. 5. Biexponential fluorescence decay of **C8-I** (1×10^{-3} M) in dichloromethane. Excitation wavelength was 340 nm.

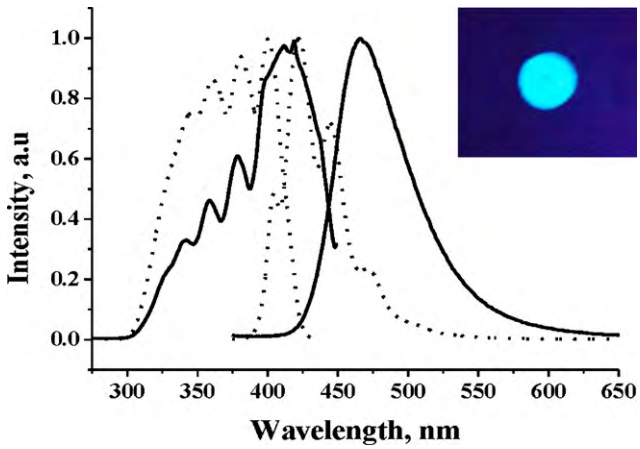

Fig. 6. Excitation (left) and emission (right) spectra of anthracene (dot) and **C18-III** (solid) at solid thin film, after heat treatment. $\lambda_{exc.}$ = 360 nm. Emission spectra are normalized to unity. Inset shows the UV illuminated photo of **C18-III** in solid thin film on a round glass slide, at room temperature, providing anthracene excimer emission.

cence decay curves for the other compounds). The shortest lifetime component of the fluorescence decays in **C8-I**, **C12-II**, **C18-III** and **PhC4-IV** possess a value of 3 ns. This decay is assigned to the emission of anthracene monomer, which is quenched by solvent collision or photoinduced electron transfer (PET) from amine to the excited state anthracene unit. The excited state lifetime component of ~7–11 ns, with relative amplitude >60–80%, was assigned to one particular type of anthracene excimer emission formed by the angular overlap of the individual anthracene units in the excited state with an angle of approximately 55°, based on literature reports [22].

The fact that more than 60% of the fluorescence decay component corresponds to the excimer emission suggests that the propensity of anthracene units to align in a columnar fashion is high even in solution phase, at concentration above 10^{-4} M. In the case of **C12-II**, an additional excited state decay component was observed with a lifetime value of ~5 ns, which is identical to the excited state decay of unquenched anthracene. Nonetheless, the relative amplitude of this lifetime component was only ~5% indicating that PET exists as a prevailing fluorescence quenching mechanism in all the compounds. Table 1 summarizes the photophysical properties of the four plastic crystals examined in the present study. Examination of Table 1 suggests that as the chain length increases, the fluorescence quantum yield decreases. This could be, presumably due to the increased flexibility of the system in the solution, introduced by the presence of long hydrocarbon chains. While the fluorescence quantum yield varies according to the chain length, the relative amplitudes of the monomer–excimer ratio remain identical within experimental error, through out the system.

3.3. *Anthracene excimer emission from the **AMA** derivatives in the plastic crystalline phase*

Next, the steady state luminescence properties of the **AMA** derivatives in the plastic crystalline phase were examined and compared with that in the crystalline phase. The plastic crystalline phase of the **AMA** derivatives was prepared through heat treatment at identical conditions adopted for POM experiments. Fig. 6 shows the excitation and emission spectra of **C18-III**, along with that of pure anthracene at identical conditions. The significant differences between the pure anthracene and **C18-III** spectra in the solid thin film are the following: (i) an additional peak appeared in the excitation spectra of **C18-III** at 412 nm, (ii) the emission maximum of **C18-III** is red-shifted to 467 nm and (iii) the emission spectra of **C18-III** is broad and structure-less. The data clearly indicates that the emission is originated purely from anthracene excimer due to the closely packed anthracene units in **C18-III**. Structure-less, broad emission from anthracene containing compounds around 470 nm indicates the presence of an excimer with angular geometry in the excited state. Identical emission spectra were obtained for other **AMA** derivatives used in the present study. The inset of Fig. 4 contains the photograph of **C18-III** under UV illumination exhibiting the anthracene excimer at ambient conditions.

The excitation and emission spectra of the **AMA** derivatives before and after the heat treatment were recorded in order to verify whether the formation of plastic crystalline phase is essential to generate the excimer emission. Fig. 7 shows the overlaid spectra of excitation and emission of **C8-I** in solid thin film before and after heat treatment. It is evident from the figure that generating **C8-I** in the plastic crystalline phase through the heat treatment facilitates the anthracene excimer formation. This is attributed to the close proximity as well as face-to-face arrangement of anthracene units in the plastic crystalline phase, which is absent in the orthorhombic crystalline phase of **C8-I**. Upon rapid cooling, the plastic crystalline phase of the **AMA** derivatives can be preserved in the glassy state, where the molecular arrangement of anthracene units remains in the face-to-face geometry. Since the intermolecular distance between the anthracene units remains at 3.9 Å in the glassy phase, excimer formation is highly feasible. Such readily formed excimers are termed as 'static excimers' since the monomer units

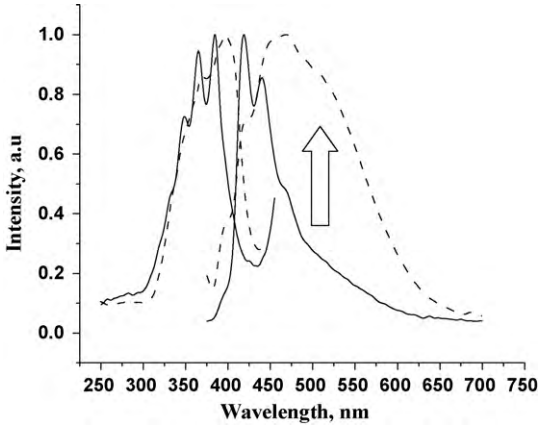

Fig. 7. Excitation (left) and emission (right) spectra of **C8-I** before (solid) and after (dash) heat treatment in solid thin film at identical experimental conditions. $\lambda_{exc.}$ = 360 nm. Intensities are normalized to unity.

are pre-arranged in the ground state in a face-to-face geometry. The static type of excimer formation is further evident from the bathochromic shift observed in the excitation spectrum shown in Fig. 7, [34]. Moreover, the absorption spectra of the **AMA** derivatives in dichloromethane (10^{-3} M) also exhibited absorbance of aggregated **AMA** derivatives at the longer wavelength of the spectrum (Supporting information Fig. S7), indicating that anthracene units in the compounds are pre-arranged in the ground state, favoring the static type excimer upon excitation [35]. The results from the photophysical studies carried out in dichloromethane and solid thin film taken together suggest that self-assembly of the **AMA** derivatives provides a simple method to generate anthracene excimer emission at room temperature, by generating static excimer of anthracene.

3.4. Preparation of in situ silver nano-clusters utilizing the *AMA* derivatives

It has been reported that stable silver nanoparticles can be generated using amphiphilic triblock copolymers arranged in hexagonal columnar phase [36]. Since the compounds **C8-I**, **C12-II**, **C18-III** and **PhC4-IV** self-assemble in rectangular columnar fashion; we have utilized them as templates for stabilizing silver nanoparticles. In general, three different methods are adopted in the literature for the preparation of silver nanoparticles from silver ions. The first one involves the radiation reduction of silver ions with γ-ray [37], ultraviolet or visible light [38], microwave [39], or ultrasound irradiation. Because of the ease of the controlling the 'on' or 'off' state of radiation, this method has attracted considerable attention. The second preparation method involves relatively strong reducing agents such as sodium borohydride [40], hydrazine, and tetrabutylammonium borohydride [41]. In the third method, silver ions were reduced by weak reducing agents, such as alcohols, through prolonged refluxing or stirring at room temperature. While reduction of silver by methanol, ethanol, glycerol etc. is feasible, these solvents alone were not able to stabilize silver nanoparticles [42,43]. Consequently, these processes have been performed in the presence of a capping agent or in microemulsions. In the present case, the third possibility (i.e., solvent induced reduction) is more likely, as the solvent (methanol) is present in bulk amount and no other reducing agents have been used for reduction. The silver nanoparticles can be stabilized by the coordination with the amine groups present in the system. While amines can also reduce silver ions [44], FT-IR studies of the system before and after nanoparticle formation clearly indicate that amine groups have not participated in any redox reactions in the present case (Supporting information S8).

All the compounds, except **PhC4-IV**, shown in Chart 1 generate nano-silver upon mixing and stirring with $AgNO_3$ for 24 h in methanol at room temperature (*vide infra*). Fig. 8 contains the UV–visible absorption spectrum of **C18-III** in the presence and absence of $AgNO_3$ in methanol. The absorption band around 500 nm, which was absent for **C18-III** alone, clearly suggests the formation of nano-silver. The plasmon absorption of nano-silver was also evident in the cases of **C8-I** and **C12-II**.

The wavelength of plasmon absorption of silver nanoparticles has been found to be strongly dependant on the size and shape of the nanoparticles formed [45]. A bathochromic shift from the blue region of the absorption spectra generally indicates the formation of larger sized metal nanoparticles [46]. Another equally important possibility is the interparticle coupling between silver nanoparticles due to the proximity effect, which increases the dielectric constant of the medium, causing the plasmon resonance maximum to shift to lower energies [47]. A third possibility is due to the formation of anisotropic metal nanoparticles in the system. According to Mie's theory, anisotropic particles could give rise to multiple

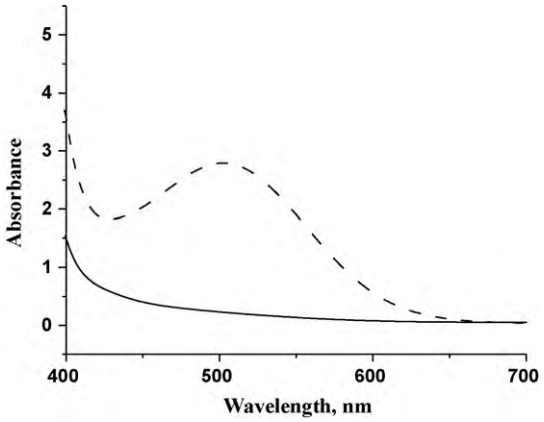

Fig. 8. UV–visible spectra of **C18-III** in the presence (dash) and absence (solid) of $AgNO_3$ in methanol.

absorption peaks in the UV–visible spectrum [48]. It is reported that absorption bands at 341 nm and 509 nm from nano-silver could be due to the formation of hexagonal nanoplates [49]. In the present cases, the absorption peaks from anthracene units mask the region below 400 nm in the spectrum, preventing further inference on the nanoparticle shape from the UV spectrum.

The silver nanosystems were further examined by scanning and transmission electron microscopic studies (SEM and TEM). Fig. 9 contains the SEM and TEM images of nano-silver generated in situ by **C18-III**. The size distribution of silver nanoparticles in **C18-III** and **C12-II** was almost similar, indicating that template effect of the **AMA** derivatives does not depend on the alkyl chain length (Supporting information Fig. S9). The nano-silver is likely to be formed in between the layers of the discotic columnar arrangements, which is stabilized through the coordination with the amines in the alkyl chains.

Since excess amount of the **AMA** derivative is present in the system, all the silver ions will likely be complexed to the amines present in the compounds. It has been reported in the literature that the reduction potential of the silver–amine complex is much lower than that of the corresponding silver ion [50]. Thus, the solvent (methanol) induced reduction of silver ions will be facilitated due to the silver–amine complex formation. The importance of the silver–amine complex formation in the reduction process of silver ions is further corroborated by the observation that no plasmon absorption was formed for the system **C8-I**/$AgNO_3$ at acidic conditions, where the amines in the system are protonated and unable to complex with the silver ions. NMR and FT-IR spectral analysis of the **AMA** derivatives after the nanoparticle formation did not exhibit any difference from the spectra taken before mixing with $AgNO_3$, indicating that amines are not participating in the reduction process. Among the four different (aminomethyl)anthracene derivatives, compound **PhC4-IV** did not generate nano-silver even after stirring with $AgNO_3$ for extended period of time. Since the nitrogen is directly attached to the electron deficient benzene ring, **PhC4-IV** is expected to be less basic compared to the other compounds used in the present study. Subsequently, the formation of the corresponding silver–amine complex would be considerably less. The poor yield of silver nanoparticles is, thus, attributed to the absence of the appreciable amount of silver–amine complex formation in the system.

3.5. Photophysical properties of the *AMA* derivatives in presence of silver nanoparticles

In order to understand whether the nano-guest particles affect the excimer formation of anthracene units in the **AMA** derivatives through reducing the proximity between the anthracene units,

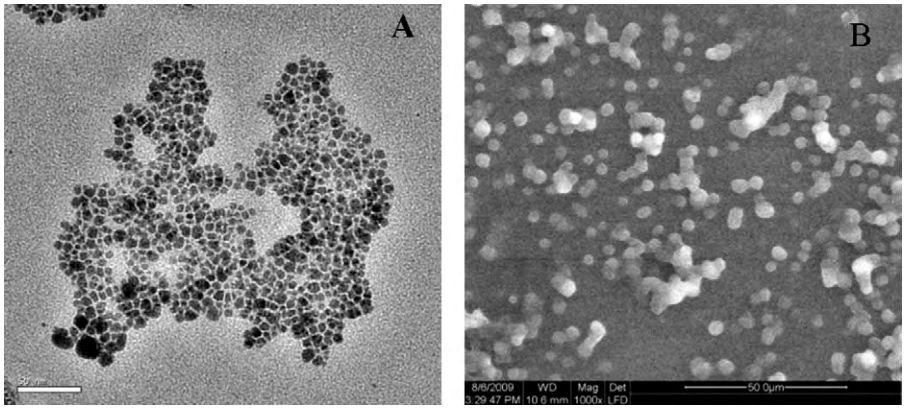

Fig. 9. (A) TEM and (B) SEM images of nano-silver generated and stabilized by the plastic crystal **C18-III** (scale = 50 μm for SEM, 50 nm for TEM).

excitation and emission spectra of the **AMA** derivatives were taken in the solid thin film after the heat treatment. Fig. 10 shows the excitation and emission spectra of **C8-I** and **C18-III** in the glassy state, in the presence and absence of silver nanoparticles.

It is clear from the figure that the presence of nanoparticles reduces the propensity of **C8-I** to generate anthracene excimer, as the emission at 470 nm is substantially decreased. This could be due to the distribution of the nano-guests in between the discotic arrangement of the molecules, creating larger separation distance between the anthracene units. POM analysis of the **AMA** derivatives in the presence of silver nanoparticles suggests a flower type arrangement (Fig. 11) for the molecular system, which also represent discotic arrangement [28]. The variations in the POM image shown in Fig. 11 compared to that in Fig. 1 indicates that anthracene units are slightly displaced from the initial arrangements. Identical behavior was observed for compound **C12-II** (Supporting information Fig. S10).

Interestingly, the presence of silver nanoparticles does not quench the excimer emission from **C18-III**, completely. The inset of Fig. 10 contains the normalized excitation and emission spectra of **C18-III** in the presence of Ag nanoparticles. This indicates that nano-guests are not able to separate the self-assembled **C18-III** molecules in the solid thin film to an extent where the excimer formation is prevented. The POM image (Supporting information Fig. S11) also corroborates this hypothesis, where the spherulitic structural pattern was clearly visible even in the presence of silver nanoparticles, indicating that structural changes in **C18-III** are marginal compared to **C8-I** and **C12-II**.

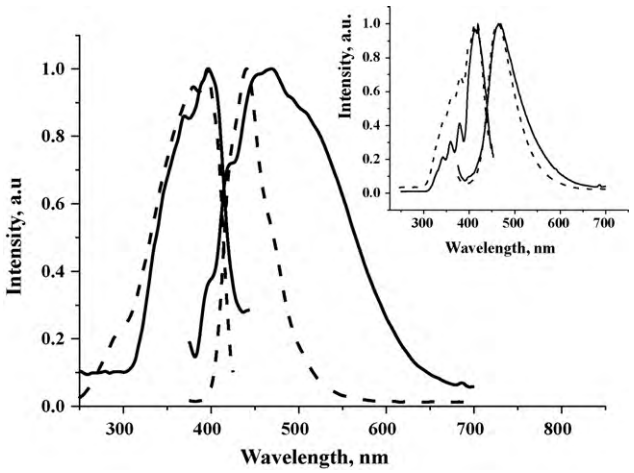

Fig. 10. Excitation (left) and emission (right) spectra of **C8-I** in the presence (dot) and absence (solid) of silver nanoparticle after heat treatment. Inset shows the same for **C18-III**, where the emission intensity is normalized. $\lambda_{exc.}$ = 360 nm.

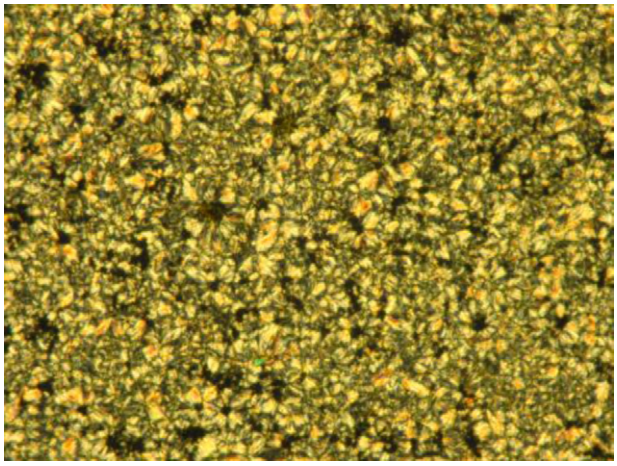

Fig. 11. Flower like texture from **C8-I** (magnification 20×). Sample for POM was prepared by making thin film of a mixture of stirred solution of **C8-I** (0.01 g, 0.03 mmol) and $AgNO_3$ (0.001 g, 0.006 mmol) in between two glass slides. The film was made uniform by heating the sample to melting followed by rapid cooling to room temperature.

The results obtained from the present study clearly suggest that the **AMA** derivatives are promising candidates for generating anthracene excimer emission at room temperature, which is a rare observation. Attempts to generate conducting molecular materials utilizing the plastic crystalline phase of the **AMA** derivatives are currently undergoing in our laboratory and the results will be published in due course.

4. Conclusion

A series of organic plastic crystals based on (aminomethyl)anthracene (**AMA**) derivatives was synthesized and the phase transitions are characterized utilizing XRD, DSC and POM. These organic plastic crystals with discotic rectangular columnar arrangement exhibit anthracene excimer emission in the solid thin film, upon exciting at 360 nm. The excimer formation is attributed to the close proximity of the anthracene units in the plastic crystalline phase, which provides the necessary condition to overlap between two anthracene units in an angular

fashion upon photoexcitation. Further investigation has shown that the silver nanoparticles can be generated and stabilized by the **AMA** derivatives, at the expense of the excimer emission intensity. Since the plastic crystalline phase can be preserved in a glassy state by rapid cooling of the system from elevated temperatures to room temperature, the experiment described here provides an easy and straight forward methodology to generate anthracene excimer emission in solid thin film at room temperature.

Acknowledgements

We thank Department of Science and Technology (SR/S1/PC-26/2007), Govt. of India for the financial support. M.J. thanks Council of Scientific and Industrial Research (CSIR), India for the fellowship. We sincerely thank Dr. Krishna Prasad, CLCR Bangalore, India for providing the XRD facility as well as fruitful discussions. Dr. T. Pradeep, IITM is acknowledged for TEM images and Department of Metallurgy, IIT M is thanked for SEM images. We thank Dr. P.K. Sudhadevi Antharjanam, Fast Track Scientist, Department of Chemistry, IIT Madras for her useful comments on the manuscript.

Appendix A. Supplementary data

Supplementary data associated with this article can be found, in the online version, at doi:10.1016/j.jphotochem.2010.07.003.

References

[1] R.M. Capito, H.S. Azevedo, Y.S. Velichko, A. Mata, S.I. Stupp, Self-assembly of large and small molecules into hierarchically ordered sacs and membranes, Science 319 (2008) 1812–1816.
[2] Y. Zhao, K. Thorkelsson, A.J. Mastroianni, T. Schilling, J.M. Luther, B.J. Rancatore, K. Matsunaga, H. Jinnai, Y. Wu, D. Poulsen, J.M.J. Fréchet, A.P. Alivisatos, T. Xu, Small-molecule-directed nanoparticle assembly towards stimuli-responsive nanocomposites, Nat. Mater. 8 (2009) 979–985.
[3] S. Varghese, N.S. Saleesh Kumar, A. Krishna, D.S. Shankar Rao, S. Krishna Prasad, S. Das, Formation of highly luminescent supramolecular architectures possessing columnar order from octupolar oxadiazole derivatives: hierarchical self-assembly from nanospheres to fibrous gels, Adv. Funct. Mater. 19 (2009) 2064–2073.
[4] B. Tuteja, M. Moniruzzaman, P.R. Sundararajan, Domains of colloidal size, mediated by self-assembly of small molecules in a polymer matrix: a three-level hierarchy of assembly, Langmuir 23 (2007) 4709–4711.
[5] Y. Zhang, W. Cao, Self-assembly of small molecules: an approach combining electrostatic self-assembly technology with host–guest chemistry, New J. Chem. 25 (2001) 483–486.
[6] M.N. Sangeetha, U. Maitra, Supramolecular gels: functions and uses, Chem. Rev. 34 (2005) 821–836.
[7] W.H. Binder, O.W. Smrzka, Self-assembly of fibers and fibrils, Angew. Chem. Int. Ed. Engl. 45 (2006) 7324–7328.
[8] K.-H. Chen, J.-S. Yang, C.-Y. Hwang, J.-M. Fang, Phospholipid-induced aggregation and anthracene excimer formation, Org. Lett. 10 (2008) 4401–4404.
[9] Y. Shiraishi, Y. Tokitoh, G. Nishimura, T. Hirai, A molecular switch with pH-controlled absolutely switchable dual-mode fluorescence, Org. Lett. 7 (2005) 2611–2614.
[10] Y. Molard, D.M. Bassani, N. Moran, J.H.R. Tucker, Structural effects on the ground and excited-state properties of photoswitchable hydrogen-bonding receptors, J. Org. Chem. 71 (2006) 8523–8531.
[11] Y. Mizobe, M. Miyata, I. Hisaki, Y. Hasegawa, N. Tohnai, Anomalous anthracene arrangement and rare excimer emission in the solid state: transcription and translation of molecular information, Org. Lett. 8 (2006) 4295–4298.
[12] Z.A. Dreger, H. Lucas, Y.M. Gupta, High pressure effects on anthracene crystals, J. Phys Chem. B 107 (2003) 9268–9274.
[13] H.B. Laurent, A. Castellen, J.-P. Desvergne, R. Lapouyade, Photodimerization of anthracenes in fluid solution: structural aspects, Chem. Soc. Rev. 29 (2000) 43–55.
[14] R.O. Al-Kaysi, A.M. Müller, C.J. Bardeen, Photochemically driven shape changes of crystalline organic nanorods, J. Am. Chem. Soc. 128 (2006) 15938–15939.
[15] T. Kobayashi, S. Nagakura, M. Szwarc, Direct observation of excimer formation in anthracene and 9,9′-bianthryl, Chem. Phys. 39 (1979) 105–110.
[16] S. Hashimoto, N. Fukazawa, H. Famumura, H. Masuhara, Observation and characterization of excimer emission from anthracene included in NaX zeolite, Chem. Phys. Lett. 219 (1994) 445–451.
[17] S. Hashimoto, S. Ikuta, T. Asahi, H. Masuhara, Fluorescence spectroscopic studies of anthracene adsorbed into zeolites: from the detection of cation–π interaction to the observation of dimers and crystals, Langmuir 14 (1998) 4284–4291.
[18] E.A. Chandross, Photolytic dissociation of dianthracene, J. Chem. Phys. 43 (1965) 4175–4176.
[19] E.A. Chandross, J. Ferguson, Photodimerization of crystalline anthracene. The photolytic dissociation of crystalline dianthracene, J. Chem. Phys. 45 (1996) 3564–3567.
[20] N. Mataga, Y. Torihashi, Y. Ota, Studies on the fluorescence decay times of anthracene and perylene excimers in rigid matrices at low temperatures in relation to the structures of excimers, Chem. Phys. Lett. 1 (1967) 385–387.
[21] J. Ferguson, A.W.-H. Mau, A spectroscopic study of the photodimerization of anthracene sandwich dimers in dianthracene, Mol. Phys. 27 (1974) 377–387.
[22] L.S. Kaanumalle, C.L.D. Gibb, B.C. Gibb, V. Ramamurthy, A hydrophobic nanocapsule controls the photophysics of aromatic molecules by suppressing their favored solution pathways, J. Am. Chem. Soc. 127 (2005) 3674–3675.
[23] G. Zhang, G. Yang, S. Wang, Q. Chen, J.S. Ma, A highly fluorescent anthracene containing hybrid material exhibiting tunable blue-green emission based on the formation of an unusual "T-shaped" excimer, Chem. Eur. J. 13 (2007) 3630–3635.
[24] R.A. Bissell, E. Calle, A.P. de Silva, H.Q.N. Gunaratne, J.-L. Habib-Jiwan, S.L.A. Peiris, R.A.D. Dayasiri Rupasinghe, T.K. Shantha, D. Samarasinghe, K.R.A. Samankumara Sandanayake, J.-P. Soumillion, Luminescence and charge transfer. Part 2. Aminomethyl anthracene derivatives as fluorescent PET (photoinduced electron transfer) sensors for protons, J. Chem. Soc., Perkin Trans. 2 (1992) 1559–1564.
[25] K. Kojima, Mechanical properties of anthracene crystals under illumination: photoplastic effects, J. Appl. Phys. 62 (1987) 1368–1375.
[26] A.B. Descalzo, D. Jimenez, M.D. Marcos, R. Martinez-Mánez, J. Soto, J.E. Haskouri, C. Guillém, D. Beltrán, P. Amorós, M.V. Borrachero, A new approach to chemosensors for anions using MCM-41 grafted with amino groups, Adv. Mater. 14 (2002) 966–969.
[27] M.R. Silva, A.M. Beja, J.A. Paixão, L.A. da Veiga, A.J.F.N. Sobral, N.G.C.L. Rebanda, A.M.d'.A.R. Gonsalves, C–H. . .π interactions in 9-(n-dodecylaminomethyl)anthracene, Acta. Cryst. C56 (2000) 1136–1138.
[28] S. Laschat, A. Baro, N. Steinke, F. Giesselmann, C. Hagele, G. Scalia, R. Judele, E. Kapatsina, S. Sauer, A. Schreivogel, M. Tosoni, Discotic liquid crystals: from tailor-made synthesis to plastic electronics, Angew. Chem. Int. Ed. Engl. 46 (2007) 4832–4887.
[29] S. Chandrasekhar, Liquid Crystals, 2nd ed., Cambridge University Press, 1993.
[30] S. Chandrasekhar, S.K. Prasad, D.S.S. Rao, V.S.K. Balagurusamy, X-ray studies on the columnar structures of discotic liquid crystals, PINSA 68 (2002) 175–191.
[31] J. Timmermans, Plastic crystals: a historical review, J. Phys. Chem. Solids 18 (1961) 1–8.
[32] J. Lenoble, N. Maringa, S. Campidelli, B. Donnio, D. Guillon, R. Deschenaux, Liquid- crystalline fullerodendrimers which display columnar phases, Org. Lett. 8 (2006) 1851–1854.
[33] J.-H. Olivier, F. Camerel, J. Barberá, P. Retailleau, R. Ziessel, Ionic liquid crystals formed by self-assembly around an anionic anthracene core, Chem. Eur. J. 15 (2009) 8163–8174.
[34] H.J. Kim, J. Hong, A. Hong, S. Ham, J.H. Lee, J.S. Kim, Cu^{2+}-induced intermolecular static excimer formation of pyrenealkylamine, Org. Lett. 10 (2008) 1963–1967.
[35] P.K. Lekha, E. Prasad, Aggregation controlled excimer emission from anthracene containing PAMAM dendrimers, Chem. Eur. J. 16 (2010) 3699–3706.
[36] L. Wang, X. Chen, J. Zhao, Z. Sui, W. Zhuang, L. Xu, C. Yang, Preparation of silver nanoparticles templated from amphiphilic block copolymer-based hexagonal liquid crystals, Colloids Surf. A: Physicochem. Eng. Aspects 257–258 (2005) 231–235.
[37] A. Henglein, M. Giersig, Formation of colloidal silver nanoparticles, J. Phys. Chem. B. 103 (1999) 9533.
[38] H.H. Huang, X.P. Ni, G.L. Loy, C.H. Chew, K.L. Tan, F.C. Loh, J.F. Deng, G.Q. Xu, Photochemical formation of silver nanoparticles in poly(N-vinylpyrrolidone), Langmuir 12 (1996) 909.
[39] F. Gao, Q.Y. Lu, S. Komarneni, Interface reaction for the self-assembly of silver nanocrystals under microwave assisted solvothermal conditions, Chem. Mater. 17 (2005) 856.
[40] S.H. Chen, K. Kimura, Water soluble silver nanoparticles functionalized with thiolate, Chem. Lett. 28 (1999) 1169.
[41] N.R. Jana, X.G. Peng, Single-phase and gram-scale routes toward nearly monodisperse Au and other noble metal nanocrystals, J. Am. Chem. Soc. 125 (2003) 14280.
[42] S. Ayyappan, R.S. Gopalan, G.N. Subbanna, C.N.R. Rao, Nanoparticles of Ag, Au, Pd, and Cu produced by alcohol reduction of the salts, J. Mater. Res. 12 (1997) 398–401.
[43] I. Pastoriza-Santos, L.M. Liz-Marzán, Formation and stabilization of silver nanoparticles through reduction by *N*,*N*-dimethylformamide, Langmuir 15 (1999) 948–951.
[44] M. Kavitha, M.R. Parida, E. Prasad, C. Vijayan, P.C. Deshmukh, Generation of Ag nanoparticles by PAMAM dendrimers and their size dependence on the aggregation behavior of dendrimers, Macromol. Chem. Phys. 210 (2009) 1310–1318.
[45] G.C. Schatz, Using theory and computation to model nanoscale properties, PNAS 104 (2007) 6885–6892.
[46] C.L. Schofield, A.H. Haines, R.A. Field, D.A. Russel, Silver and gold nanoparticles for colorimetric bioassays, Langmuir 22 (2006) 6707–6711.

[47] Z.V. Saponjic, R. Csencsits, T. Rajh, N.M. Dimitrijevic, Self-assembly of TOPO-derivatized silver nanoparticles into multilayered film, Chem. Mater. 15 (2003) 4521–4526.
[48] M. Maillard, M.-P. Pileni, S. Link, M.A. El-Sayed, Pico second self-induced thermal lensing from colloidal silver nanodisks, J. Phys. Chem. B 108 (2004) 5230–5234.
[49] J. An, B. Tang, X. Ning, J. Zhou, S. Xu, B. Zhao, W. Xu, C. Corredor, J.R. Lombardi, Photoinduced shape evolution: from triangular to hexagonal silver nanoplates, J. Phys. Chem. C 111 (2007) 18055–18059.
[50] G. Maduraiveeran, R. Ramraj, Potential sensing platform of silver nanoparticles embedded in functionalized silicate shell for nitroaromatic compounds, Anal. Chem. 81 (2009) 7552–7560.